RSC Advances

PAPER

View Article Online
View Journal | View Issue

Open Access Article. Published on 22 July 2021. Downloaded on 10/26/2025 4:56:00 PM.
This article is licensed under a Creative Commons Attribution-NonCommercial 3.0 Unported Licence.

Check for updates

Cite this: *RSC Adv.*, 2021, **11**, 25524

The molecular imprinting of magnetic nanoparticles with boric acid affinity for the selective recognition and isolation of glycoproteins†

Bangjin Wang,[a] Aihong Duan,[a] Shengming Xie,[a] Junhui Zhang,[a] Liming Yuan*[a] and Qiue Cao*[b]

A strategy was designed for the molecular imprinting of magnetic nanoparticles with boric acid affinity (MNPs@MIP) which were then used for the selective recognition and isolation of glycoproteins. Fe_3O_4 nanoparticles were prepared by a solvothermal method and direct silanization by the condensation polymerization of aminopropyltriethoxysilane (APTES). Subsequently, phenylboric acid was functionalized by reductive amination between 2,3-difluoro-4-formyl phenylboric acid (DFFPBA) and the amido group. The resultant Fe_3O_4@SiO_2–DFFPBA was then used for the selective adsorption of a glycoprotein template. Finally, a molecularly imprinted layer was covered on the surface nanoparticles by the condensation polymerization of tetraethyl orthosilicate (TEOS). The adsorption capacities of the resultant MNPs@MIP–HRP and MNPs@MIP–OVA to horseradish peroxidase (HRP) or ovalbumin (OVA) were significantly higher than non-imprinted particles (MNPs@NIP). Moreover, the adsorption capacities of MNPs@MIP–HRP and MNPs@MIP–OVA on non-template protein and non-glycoprotein bovine serum albumin (BSA) were significantly lower than those of their respective template proteins, thus indicating that both of the prepared MNPs@MIP exhibited excellent selectivity.

Received 27th January 2021
Accepted 18th July 2021

DOI: 10.1039/d1ra00716e

rsc.li/rsc-advances

Introduction

The glycosylation of proteins is one of the most important post-translational modification processes in living organisms. As such, glycoproteins play an important role in many biological pathways, including molecular recognition, cell adhesion and immune response.[1–4] More importantly, the improper expression of glycoproteins is closely related to many diseases, including cancer[5–7] and neurodegenerative diseases.[8–10] Therefore, the specific identification and isolation of glycoproteins has become a significant field of research.

At present, materials based on lectin,[11] antibodies,[12] and hydrazine chemistry[13] are used for the selective recognition and isolation of glycoproteins. Of these three types of materials, lectin has numerous advantages in terms of material variety; however, its stability and specific recognition ability for glycoprotein are worse than the other two types of materials. Antibodies have the highest specificity for recognizing glycoproteins, but they are also the most expensive. The glycoprotein enrichment efficiency of materials created by hydrazide chemistry is the best, although the procedure needed to prepare these materials is complicated and the conditions required are not easy to control.

Previous research has found that boric acid can selectively adsorb glycoproteins by forming five or six membered cyclic esters between boric acid and the *cis*-diol of glycosyl.[14,15] Furthermore, it is possible to regulate the adsorption and desorption processes by simply adjusting the pH value.[16,17] Therefore, boric acid affinity has become widely applied for the recognition and separation of glycoproteins.[17–22] Subsequent research has demonstrated that molecularly imprinted materials based on boric acid affinity can exhibit an excellent capacity for selectivity and adsorption.[23–26]

In the present study, the high selectivity of boric acid affinity molecular imprinting technology was combined with the rapid separation and reusability of magnetic nanomaterials to achieve the specific recognition and rapid separation of glycoproteins.

Experimental

Reagents and material

Horseradish peroxidase (HRP) was obtained from MeilunBio (Dalian, China). 3-Aminopropyltriethoxysilane (APTES), 2,3-

[a]Department of Chemistry, Yunnan Normal University, Kunming 650500, China
[b]Key Laboratory of Medicinal Chemistry for Natural Resource, Ministry of Education, School of Chemical Science and Technology, Yunnan University, Kunming 650091, China

† Electronic supplementary information (ESI) available. See DOI: 10.1039/d1ra00716e

© 2021 The Author(s). Published by the Royal Society of Chemistry

Open Access Article. Published on 22 July 2021. Downloaded on 10/26/2025 4:56:00 PM.
This article is licensed under a Creative Commons Attribution-NonCommercial 3.0 Unported Licence.

difluoro-4-formyl phenylboric acid (DFFPBA), and tetraethyl orthosilicate (TEOS), were purchased from Sigma-Aldrich (St. Louis, MO, USA). Bovine serum albumin (BSA), transferrin (TRF), and ovalbumin (OVA), were obtained from Aladdin (Shanghai, China). All reagents were used without further purification. Deionised water was used to prepare all buffer and analyte solutions.

General procedure for the synthesis of MNPs@MIP–glycoprotein

The general scheme for the synthesis of MNPs@MIP–glycoprotein is illustrated in Fig. 1. The Fe_3O_4 nanoparticles were synthesized by the solvothermal method,[27] and a direct silanizing method with APTES was used for the amino group functionalization of Fe_3O_4 nanoparticles.[28] Subsequently, we obtained functionalized phenylboric acid by the reductive amination between 2,3-difluoro-4-formyl phenylboric acid (DFFPBA) and the amido group.[29] The resultant Fe_3O_4@SiO_2–DFFPBA was used for the selective adsorption of a template glycoprotein. Finally, the imprinted layer was formed by a sol–gel process of TEOS on the surface using nanoparticles.

Binding experiments

Adsorption capacity. The adsorption capacity of MNPs@MIP–glycoprotein was investigated using a static adsorption method.

To begin with, 2.0 mg Fe_3O_4@SiO_2–FFPBA or MNPs@MIP–glycoprotein were dispersed by ultrasound in 200 μL of test solution (1.0 mg mL^{-1}) which was prepared using an ammonium bicarbonate buffer solution at a concentration of 50 mM (pH = 8.5, containing 500 mM NaCl) with shaking at room temperature (1200 rpm) for 2 h. The concentration of the test solution after adsorption was obtained by determining the ultraviolet absorbance. Then the adsorption capacity (Q_e) was calculated using eqn (1).

$$Q_e = \frac{V(C_0 - C_e)}{m} \times 1000 \quad (1)$$

In eqn (1), C_0 (mg mL^{-1}) represents the initial concentration of protein solution, C_e (mg mL^{-1}) represents the equilibrium concentration of the protein, V (ml) represents the volume of the protein solution, and m (mg) represents the mass of MNPs@MIP–glycoprotein. Contrast adsorption experiments were also performed with MNPs@NIP under the same conditions.

Thermodynamics and the kinetics of adsorption

Isothermal adsorption experiments were carried out as follows. MNPs@MIP–glycoprotein were added to test solution (0.1 to 1.0 mg mL^{-1}) and shaken at room temperature (1200 rpm) for 60 min. The Scatchard equation was then employed to investigate the binding properties of the MNPs@MIP–glycoprotein and MNPs@NIP, as shown by eqn (2).

$$\frac{Q}{C} = \frac{(Q_{max} - Q)}{K_D} \quad (2)$$

In eqn (2), Q (mg g^{-1}) represents the equilibrium adsorption capacity of the material to the substrate, C (mg mL^{-1}) represents the substrate concentration remaining in the adsorption solution after adsorption equilibrium, Q_{max} (mg g^{-1}) represents the maximum apparent binding amount, and K_D represents the equilibrium dissociation constant.

For the kinetics adsorption experiments, the shaking time was changed from 20 min to 140 min. The concentration of the test solutions was kept constant at 1.0 mg mL^{-1}.

Selectivity experiments

The selectivities of the MNPs@MIP–OVA or MNPs@MIP–HRP, and MNPs@NIP were evaluated using OVA, HRP, BSA, and TRF (1.0 mg mL^{-1}) as competitors. The imprinting factor (IF) was used to estimate the recognition capability according to eqn (3).

$$IF = \frac{Q_{MIP}}{Q_{NIP}} \quad (3)$$

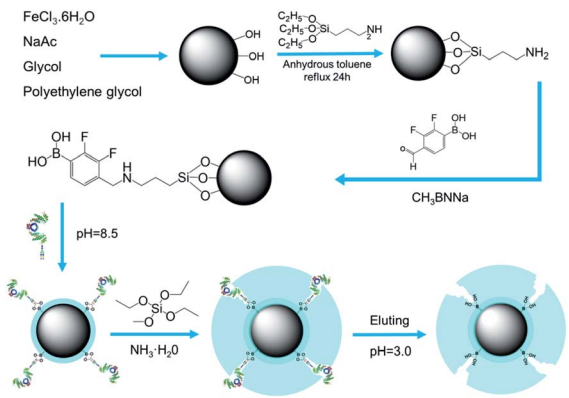

Fig. 1 The synthetic routes used to produce boric acid affinity magnetic nano-molecularly imprinted particles.

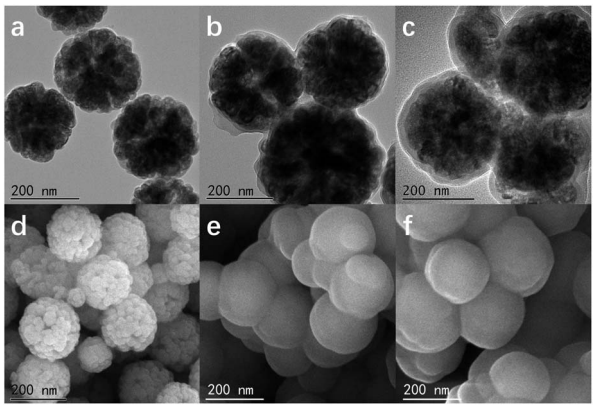

Fig. 2 Transmission electron microscope images (a–c) and scanning electron microscope images (d–f) of Fe_3O_4 (a and d), Fe_3O_4@APTES (b and e) and MNPs@MIP (c and f).

Open Access Article. Published on 22 July 2021. Downloaded on 10/26/2025 4:56:00 PM.
This article is licensed under a Creative Commons Attribution-NonCommercial 3.0 Unported Licence.

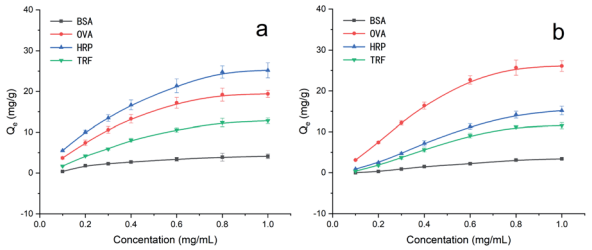

Fig. 3 Adsorption isothermal curves for (a) MNPs@MIP–HRP and (b) MNPs@MIP–OVA.

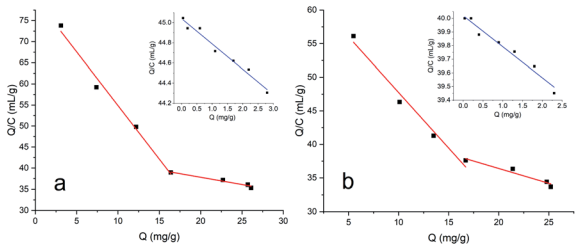

Fig. 4 Scatchard curve for MNPs@MIP-HRP to HRP (inset: the Scatchard curve for MNPs@NIP to HRP) (a) and MNPs@MIP–OVA to OVA (inset: the Scatchard curve for MNPs@NIP to OVA) (b).

In eqn (3), Q_{MIP} and Q_{NIP} represent the adsorption amounts of the template or the competitive proteins on the MNPs@MIP–OVA or MNPs@MIP–HRP and MNPs@NIP, respectively.

Results and discussion

Characterization of MNPs@MIP

The morphology of the prepared materials was analysed by transmission electron microscopy (TEM) and scanning electron microscopy (SEM). As shown in Fig. 2a and d, the Fe_3O_4 nanoparticles were 200 nm in diameter and were self-assembled from smaller particles with a diameter of approximately 10 nm. Fig. 2b and e show that the nanoparticles were modified by APTES coating (Fe_3O_4@SiO_2–NH_2). On the surface of the particles, we observed a 5 nm layer of silicon dioxide coating containing an ammonia propyl group (Fig. 2b). The new silicon dioxide imprinting layer also increased the thickness of the silicon dioxide coating layer (Fig. 2c). Due to the silicon dioxide coating, the interstices on the surface of the Fe_3O_4 particles could not be observed clearly (Fig. 2e and f).

The distribution of the different elements of Fe_3O_4@SiO_2–FFPBA was observed under a scanning transmission electron microscope (STEM). Fig. S1† shows that the distribution of Fe, O, F, Si, and N, were very clear and were highly consistent with the contours of the particles, thus indicating that aminopropyl silane had been successfully coated on the surface of the particles. Although the distribution of boron did not appear to be clear, the presence of fluorine (which also forms the molecular structure of 2,3-difluoro-4-formylbenzene boric acid), provides strong evidence that phenylboric acid had been successfully added to the surface of the particles.

The distribution of elements in Fe_3O_4@SiO_2–FFPBA was also confirmed by X-ray photoelectron spectroscopy (XPS), in addition to its specific composition. As shown in Fig. S2,† the presence of a characteristic nitrogen peak at 398.4 eV and a silicon peak at 150.5 eV indicated that aminopropyl silane had been successfully coated on to the surface of the particles. Furthermore, the successful modification of 2,3-difluoro-4-formylbenzene boric acid was confirmed by the appearance of a boron peak at 191.4 eV and a fluorine peak at 685.7 eV.

Further evidence to support the successful modification of our nanoparticles was acquired from thermogravimetric analysis (TGA) curves. Fig. S3† shows that the Fe_3O_4 nanoparticles did not experience a significant loss of weight at high temperatures. However, with the introduction of ammonia propyl and phenylboronic acid groups, the Fe_3O_4@SiO_2–NH_2 and Fe_3O_4@SiO_2–FFPBA experienced a gradual loss of weight.

Data acquired by the vibration sample magnetometer (VSM) from the Fe_3O_4 nanoparticles, Fe_3O_4@SiO_2–FFPBA, and MNPs@MIP are shown in Fig. S4.† None of these products showed any obvious coercivity or hysteresis loops at room temperature, thus indicating typical super-paramagnetism.

Optimization of the thickness of the imprinted layer

In order to investigate how the thickness of the imprinted layer influenced adsorption capacity, we investigated two direct influencing factors: the amount of ammonia (from 0.2 to 1.2 mL) and the reaction time (from 10 to 60 min). TEM images acquired from the MNPs@MIP are shown in Fig. S5 and S6.† These images show that the thickness of the imprinted layer was significantly increased when the dose of ammonia was increased or when the reaction time was prolonged. The

Table 1 Scatchard plot analysis for MNPs@MIP–HRP and MNPs@MIP–OVA

Metarials	Affinity of binding sites	Substrates	r^2	Q_{max} (mg g^{-1})	K_D (mg mL^{-1})
MNPs@MIP–HRP	High	HRP	0.9885	31.48	0.39
	Low	HRP	0.9612	131.45	2.94
MNPs@NIP	Low	HRP	0.9739	160.20	4.00
MNPs@MIP–OVA	High	OVA	0.9804	38.72	0.60
	Low	OVA	0.9432	102.72	2.27
MNPs@NIP	Low	OVA	0.9674	174.09	4.35

 © 2021 The Author(s). Published by the Royal Society of Chemistry

Open Access Article. Published on 22 July 2021. Downloaded on 10/26/2025 4:56:00 PM.
This article is licensed under a Creative Commons Attribution-NonCommercial 3.0 Unported Licence.

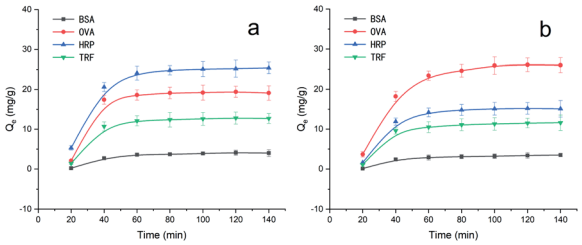

Fig. 5 Kinetics adsorption curves for (a) MNPs@MIP–HRP and (b) MNPs@MIP–OVA.

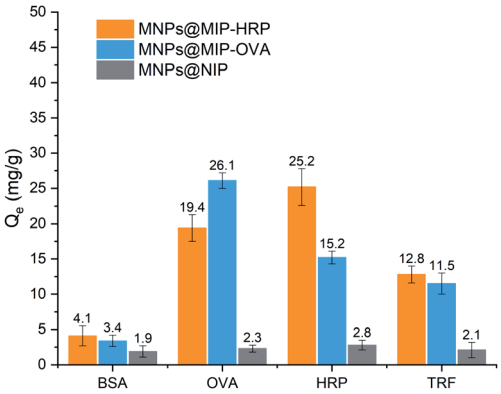

Fig. 6 The adsorption capacity of different materials to BSA, OVA, HRP and TRF when present alone.

adsorption capacity of an imprinted material depends on the number of binding sites on the surface of the material. Consequently, the thinner imprinted layer exposed more binding sites and led to a higher adsorption capacity (Fig. S7†). However, a thinner imprinted layer prevented the formation of imprinted cavities and reduced selectivity. Therefore, 0.4 mL of ammonia and a reaction time of 30 min, were used to prepare MNPs@MIP–OVA. In contrast, 0.4 mL of ammonia and a reaction time of 40 min was used to prepare MNPs@MIP–HRP.

The binding properties of MNPs@MIP

As shown in Fig. 3, the adsorption capacity of MNPs@MIP–HRP and MNPs@MIP–OVA increased rapidly with increasing concentrations of HRP or OVA (from 0.1 to 1.0 mg mL^{-1}) and achieved saturation at a concentration of 1.0 mg mL^{-1}. Therefore, a concentration of 1.0 mg mL^{-1} was selected as the optimum concentration in the subsequent experiments.

Data derived from Scatchard analysis is shown in Fig. 4 and Table 1. As shown in Fig. 4, the MNPs@MIP exhibited a much stronger affinity towards glycoproteins than to the MNPs@NIP. Moreover, data shown in Table 1 indicate that two binding sites (with high affinity and low affinity), existed on the surface of MNPs@MIP. In contrast, only low affinity binding sites were found on the surface of the MNPs@NIP. Compared with the low affinity sites, the high affinity sites showed a lower equilibrium dissociation constant (K_D), further indicating that the presence of boric acid leads to a stronger affinity for glycoproteins.

Next, we investigated the binding rate of MNPs@MIP–HRP and MNPs@MIP–OVA. Therefore, we conducted binding kinetics experiments using 1.0 mg mL^{-1} HRP or OVA solution at different time intervals from 20 to 140 min; the results are presented in Fig. 5. We observed that both MNPs@MIP–HRP and MNPs@MIP–OVA were associated with a fast adsorption profile and that the adsorption equilibrium was reached after 80 min and 100 min, respectively.

Selectivity

Fig. 6 shows the adsorption capacity of MNPs@MIP–HRP, MNPs@MIP–OVA, and MNPs@-NIP for BSA, OVA, HRP, and TRF. It was evident that MNPs@MIP–HRP and MNPs@MIP–OVA had higher adsorption capacities for glycoproteins when compared to non-glycoprotein BSA, thus revealing excellent selectivity. Moreover, both of these materials had a higher adsorption capacity than the other glycoproteins for their respective template molecules, thus demonstrating good recognition specificity. Fig. 6 also shows that the adsorption capacity of MNPS–NIP to proteins was significantly lower than for MNPs@MIP–HRP and MNPs@MIP–OVA, and there was no

Table 2 The adsorption capacity (Q_e) and imprinting factor (IF) of other molecularly imprinted materials based on boric acid affinity, as reported in the recent literature

Adsorbent	Adsorbate	Q_e (mg g^{-1})	IF	References
GO–APBA/MIPs–OVA	OVA	278.0	9.60	30
GO–APBA/MIPs–HRP	HRP	218.75	6.73	30
MNPs@pTiO$_2$@MIP–OVA	OVA	30.75	1.35	31
MNPs@pTiO$_2$@MIP–HRP	HRP	69.04	3.37	31
MMINs	OVA	30.6	3.58	32
MMINs	HRP	49.6	6.20	32
Fe_3O_4@PGMA–TBA/MIPs	OVA	190.7	7.37	33
GO@PVPBA	OVA	514.8	—	34
Fe_3O_4@P(AAPBA-*co*-PEGMA)	OVA	340.0	—	35
CPBA-Ni_6PW_9/SA	OVA	373.3	—	36
MCNTs@p(PEGMA-*co*-VPBA)	HRP	51.0	—	37
MNPs@MIP–HRP	HRP	25.2	12.43	This work
MNPs@MIP–OVA	OVA	26.1	10.96	This work

Open Access Article. Published on 22 July 2021. Downloaded on 10/26/2025 4:56:00 PM.
This article is licensed under a Creative Commons Attribution-NonCommercial 3.0 Unported Licence.

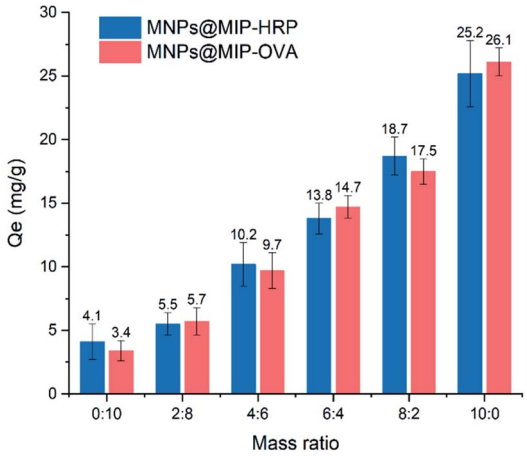

Fig. 7 Adsorption capacity of MNPs@MIP–OVA and MNPs@MIP–HRP to the mixed samples containing different mass ratios of non-glycoprotein BSA and glycoprotein HRP or OVA.

selectivity for glycoproteins and non-glycoproteins. These data indicated that both MNPs@MIP had a high imprinting effect, with imprinting factors (IF) of 10.96 and 12.42, respectively. Compared with other molecularly imprinted materials based on boric acid affinity, as reported in the recent literature[30–37] (Table 2), the imprinted materials prepared in the current study had a lower adsorption capacity for template glycoprotein, but they also had the highest imprinting factor, thus indicating that they exhibited better selectivity to template glycoprotein.

Adsorption experiments on mixed samples containing different mass ratios of non-glycoprotein BSA and glycoprotein HRP or OVA were conducted to further investigate the adsorption selectivity of MNPs@MIP–OVA and MNPs@MIP–HRP (Fig. 7). The results showed that the adsorption capacity of the two MNPs@MIP to the eluent increased with the increase of the mass proportion of template glycoprotein in the mixed solution, which verified the selective adsorption capacity of MNPs@MIP–OVA and MNPs@MIP–HRP to the template glycoprotein.

MALD-TOF was used to detect the solution prior to adsorption, and the eluent after adsorption by MNPs@MIP and MNPs@NIP; the results are shown in Fig. 8. It was evident that the content of template proteins in the eluent following the adsorption of MNPs@MIP was significantly higher than that after the adsorption of MNPs@NIP, thus indicating that the resultant MNPs@MIP had excellent selectivity for template proteins.

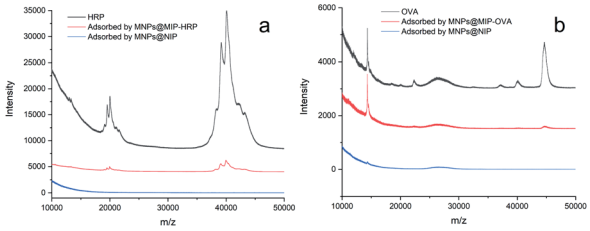

Fig. 8 MALDI-TOF MS spectra of the solution before adsorption and the eluent adsorbed by MNPs@MIP and MNPs@NIP: (a) HRP, (b) OVA.

Reusability

Next, we tested the reusability of MNPs@MIP and obtained satisfying results (Fig. S8†). Due to the loss of imprinted particles during the recycling process, the adsorption capacity of MNPs@MIP–OVA and MNPs@MIP–HRP decreased slightly after five adsorption–desorption cycles. These results suggest that the stability of MNPs@MIP is satisfactory and that this material can be used in practical applications.

Conclusions

In summary, we designed a novel strategy for the assembly of magnetic nanoparticles that were molecularly imprinted with boric acid affinity. This was achieved by the direct silanizing method, the reductive amination method, and the sol–gel method. The resultant MNPs@MIP exhibited high adsorption capacity and excellent reusability. In addition, the selective recognition and isolation of glycoproteins was successfully achieved. The combination of direct silanization, reductive amination and the sol–gel process, is a feasible strategy with which to assemble magnetic nanoparticles molecularly imprinted with boric acid affinity that can be used to recognize and isolate glycoproteins.

Conflicts of interest

There are no conflicts to declare.

Acknowledgements

This research was supported by the National Natural Science Foundation of China (No. 91856123 and No. 21665028).

Notes and references

1 K. Ohtsubo and J. D. Marth, *Cell*, 2006, **126**, 855–867.
2 R. J. Copeland, G. Han and G. W. Hart, *Proteomics: Clin. Appl.*, 2013, **7**, 597–606.
3 A. Helenius and M. Aebi, *Annu. Rev. Biochem.*, 2004, **73**, 1019–1049.
4 A. Lux and F. Nimmerjahn, *Adv. Exp. Med. Biol.*, 2011, **780**, 113–124.
5 L. Uttley, B. L. Whiteman, H. B. Woods, S. Harnan, S. T. Philips, I. A. Cree and C. Early, Cancer Detection, *EBioMedicine*, 2016, **10**, 164–173.
6 D. H. Dube and C. R. Bertozzi, *Nat. Rev. Drug Discovery*, 2005, **4**, 477–488.
7 M. M. Fuster and J. D. Esko, *Nat. Rev. Cancer*, 2005, **5**, 526–542.
8 H. Hwang, J. Zhang, K. A. Chung, J. B. Leverenz, C. P. Zabetian, E. R. Peskind, J. Jankovic, Z. Su, A. M. Hancock, C. Pan, T. J. Montine, S. Pan, J. Nutt, R. Albin, M. Gearing, R. P. Beyer, M. Shi and J. Zhang, *Mass Spectrom. Rev.*, 2010, **29**, 79–125.
9 A. Palmigiano, R. Barone, L. Sturiale, C. Sanfilippo, R. O. Bua, D. A. Romeo, A. Messina, M. L. Capuana,

 © 2021 The Author(s). Published by the Royal Society of Chemistry

Open Access Article. Published on 22 July 2021. Downloaded on 10/26/2025 4:56:00 PM.
This article is licensed under a Creative Commons Attribution-NonCommercial 3.0 Unported Licence.

T. Maci, F. Le Pira, M. Zappia and D. Garozzo, *J. Proteomics*, 2016, **131**, 29–37.
10 S. Schedin-Weiss, B. Winblad and L. O. Tjernberg, *FEBS J.*, 2014, **281**, 46–62.
11 B. F. Mann, A. K. P. Mann, S. E. Skrabalak and M. V. Novotny, *Anal. Chem.*, 2013, **85**, 1905–1912.
12 P. C. Lin, P. H. Chou, S. H. Chen, H. K. Liao, K. Y. Wang, Y. J. Chen and C. C. Lin, *Small*, 2006, **2**, 485–489.
13 J. Huang, H. Wan, Y. Yao, J. Li, K. Cheng, J. Mao, J. Chen, Y. Wang, H. Qin, W. Zhang, M. Ye and H. Zou, *Anal. Chem.*, 2015, **87**, 10199–10204.
14 W. L. Brooks and B. S. Sumerlin, *Chem. Rev.*, 2016, **116**, 1375–1397.
15 R. Nishiyabu, Y. Kubo, T. D. James and J. S. Fossey, *Chem. Commun.*, 2011, **47**, 1106–1123.
16 D. J. Li, Y. Chen and Z. Liu, *Chem. Soc. Rev.*, 2015, **44**, 8097–8123.
17 Z. Liu and H. He, *Acc. Chem. Res.*, 2017, **50**, 2185–2193.
18 C. Bi, S. Zhang, Y. Li, X. He, L. Chen and Y. Zhang, *New J. Chem.*, 2018, **42**, 17331–17338.
19 X. Zhang, X. He, L. Chen and Y. Zhang, *J. Mater. Chem.*, 2012, **22**, 16520–16526.
20 Y. Liu, Y. Lu and Z. Liu, *Chem. Sci.*, 2012, **3**, 1467.
21 J. Liu, K. Yang, W. Shao, Y. Qu, S. Li, Q. Wu, L. Zhang and Y. Zhang, *ACS Appl. Mater. Interfaces*, 2016, **8**, 9552–9556.
22 Y. Wang, X. Hai, S. E, M. Chen, T. Yang and J. Wang, *Nanoscale*, 2018, **10**, 4913–4920.
23 X. Wang, J. Yu, Q. Kang, D. Shen, J. Li and L. Chen, *Biosens. Bioelectron.*, 2016, **77**, 624–630.
24 W. Wan, Q. Han, X. Zhang, Y. Xie, J. Sun and M. Ding, *Chem. Commun.*, 2015, **51**, 3541–3544.
25 J. Erdőssy, V. Horváth, A. Yarman, F. W. Scheller and R. E. Gyurcsányi, *TrAC, Trends Anal. Chem.*, 2016, **79**, 179–190.
26 A. Pal, M. Berube and D. G. Hall, *Angew. Chem., Int. Ed. Engl.*, 2010, **49**, 1492–1495.
27 H. Deng, L. X. Lin, P. Qing, X. Wang, J. P. Chen and Y. D. Li, *Angew. Chem., Int. Ed.*, 2005, **44**, 2782–2785.
28 X. Kan, Q. Zhao, D. Shao, Z. Geng, Z. Wang and J. J. Zhu, *J. Phys. Chem. B*, 2010, **114**, 3999–4004.
29 Z. J. Bie, Y. Chen, J. Ye, S. S. Wang and Z. Liu, *Angew. Chem., Int. Ed. Engl.*, 2015, **54**, 10211–10215.
30 J. Luo, J. Huang, J. J. Cong, W. Wei and X. Y. Liu, *ACS Appl. Mater. Interfaces*, 2017, **9**, 7735–7744.
31 X. Y. Sun, R. T. Ma, J. Chen and Y. P. Shi, *Mikrochim. Acta*, 2018, **185**, 565–574.
32 R. T. Ma, W. Ha, J. Chen and Y. P. Shi, *J. Mater. Chem. B*, 2016, **4**, 2620–2627.
33 H. Zhu, H. Yao, K. Xia, J. Liu, X. Yin, W. Zhang and J. Pan, *Chem. Eng. J.*, 2018, **346**, 317–328.
34 X. An, X. He, L. Chen and Y. Zhang, *J. Mater. Chem. B*, 2016, **4**, 6125–6133.
35 X. H. Zhang, J. W. Wang, X. W. He, L. X. Chen and Y. K. Zhang, *ACS Appl. Mater. Interfaces*, 2015, **7**, 24576–24584.
36 W. Xu, J. F. Cao, Y. Y. Zhang, Y. Shu and J. H. Wang, *Talanta*, 2020, **210**, 120620.
37 X. An, H. Wu, Y. Li, X. He, L. Chen and Y. Zhang, *Talanta*, 2020, **210**, 120632.

© 2021 The Author(s). Published by the Royal Society of Chemistry